

Adsorption of phosphate on magnetite-enriched particles (MEP) separated from the mill scale

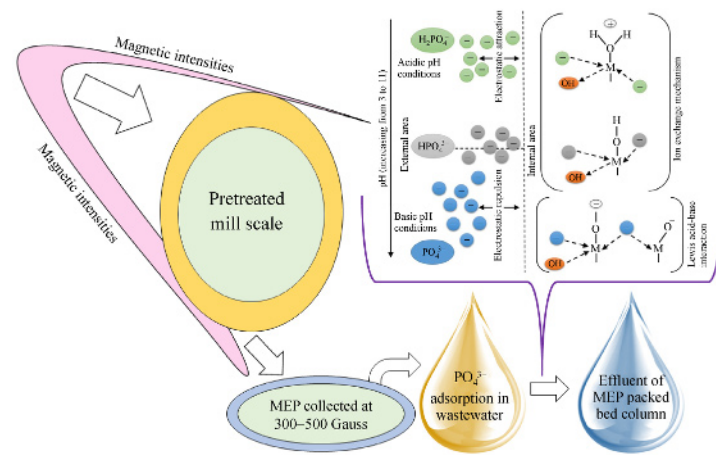
Muhammad Kashif Shahid¹, Yunjung Kim², Young-Gyun Choi (✉)¹

1 Department of Environmental Engineering, Chungnam National University, Daejeon 34134, Republic of Korea
2 Mechanical Process Research Group, Engineering Center, POSCO E&C, Incheon 220099, Republic of Korea

HIGHLIGHTS

- MEP were separated from mill scale at low magnetic intensity i.e., 300 to 500 gauss.
- The phosphate adsorption capacity of MEP was determined 6.41 mg/g.
- MEP packed-bed columns were successfully regenerated with alkaline solution.

GRAPHIC ABSTRACT



ARTICLE INFO

Article history:

Received 19 April 2019

Revised 26 June 2019

Accepted 5 July 2019

Available online 9 August 2019

Keywords:

Adsorption
Magnetite
Mill-scale
Phosphate
Wastewater treatment

ABSTRACT

Phosphate is a major pollutant in water, causing serious environmental and health consequences. In present study, the phosphate adsorption on novel magnetite-enriched particles (MEP) was comprehensively investigated. A new method and device were introduced for the separation of MEP from the mill scale at low magnetic intensity. Particles were characterized with different techniques such as XRD, XRF, SEM and EDS. The XRD and XRF analysis of MEP identified the dominant existence of crystalline magnetite. Furthermore, the morphological analysis of MEP confirmed the agglomerate porous morphology of magnetite. Oxygen and iron, the main constituents of magnetite were acknowledged during the elemental analysis using EDS. The phosphate adsorption on MEP is well explained using various isotherm and kinetic models, exhibiting the monolayer adsorption of phosphate on the surface of MEP. The maximum adsorption capacity was determined 6.41 mg/g. Based on particle size (45–75 and 75–150 μm) and empty bed contact time (1 and 2 h), four columns were operated for 54 days. MEP were appeared successful to remove all phosphate concentration from the column influent having 2 mg/L concentration. The operated column reactors were successfully regenerated with alkaline solution. The results indicated potential for practical application of the MEP for phosphate removal.

© Higher Education Press and Springer-Verlag GmbH Germany, part of Springer Nature 2019

1 Introduction

Phosphorus is an essential nutrient found in natural ecosystem. The growth of organisms in most of the

ecosystems highly depends on phosphorus contents. Depending on the pH, an orthophosphoric acid can be found in the form of H_3PO_4 , H_2PO_4^- , HPO_4^{2-} and PO_4^{3-} (Nohra et al., 2007). Among all the orthophosphoric species, PO_4^{3-} has the strong affinity for covalent bonding with the functional group of soil. Hence, it is most targeted specie in nutrient recovery. The decomposition of rocks and minerals, sedimentation, erosion, atmospheric deposi-

✉ Corresponding author

E-mail: youngchoi@cnu.ac.kr

tion and direct contribution by animals are the known natural sources of phosphate in aquatic environment (Vikrant et al., 2018). An effluent from the agricultural and industrial units also carries high concentration of phosphorus that may results in eutrophication of the aquatic environment and health concerns (Li et al., 2017). Therefore, control measures are always required for phosphate concentration in wastewater. Various methods are known for the removal of phosphate and other contaminates from the water such as membrane technology, chemical precipitation, electrocoagulation, biological treatment and adsorption (Huang et al., 2017; Shahid et al., 2017; Li et al., 2018; Shahid et al., 2018b).

Each phosphate remediation method has its own advantages and disadvantages. Membrane treatment is found more effective method to remove phosphate in comparison with others. However, bulk consumption of energy does not make it economically viable. Moreover, the inorganic scale deposition is also a challenging issue in membrane treatment (Ngo and Guo, 2009; Shahid and Choi, 2018). The pH, fluctuant temperature and chemical oxygen demand seriously affect the biological treatment process. However, water purification with adsorbents seems more successful and economical. Adsorption process involves the accumulation of contaminants (adsorbate) on the surface of adsorbent, normally solid phase. Water remediation by adsorption is always optimized using different dynamics i.e., particle size of adsorbent, adsorbate concentration into the solution, pH, temperature, amount of adsorbent, nature of adsorbent and adsorbate, coexisting ions in water and flowrate in case of continuous reactor operation. Various adsorbents are known for the treatment of contaminated water (Khafri et al., 2017; Shahid et al., 2019a). Among other adsorbents, metal oxides are well known for the adsorption of phosphate (Ye et al., 2017; Gypser et al., 2018; Zhang et al., 2018). The oxides of iron, especially magnetite has been used for adsorptive removal of phosphate due to its high surface area, micro and mesoporous morphology and good adsorption capacity (Rashid et al., 2017; Guaya et al., 2018).

In this study, a novel method was presented for the separation of magnetite-enriched particles (MEP) from the mill scale at low magnetic intensities. Particles were further used for phosphate recovery from the contaminated water. A new device was introduced for the separation of MEP. The applied method and device were never used before for the separation of magnetite from the mill scale or any other mixture of iron oxides. In our earlier study, we synthesized magnetite particles from the mill scale by coprecipitation of $\text{Fe}^{2+}/\text{Fe}^{3+}$ in alkaline environment (Shahid et al., 2018a; Shahid et al., 2019b). Unlike coprecipitation method, the proposed method in this study, eliminated the consumption of chemicals during MEP synthesis. The novel MEP were characterized with advanced instruments to understand their morphological,

chemical and physical characteristics. The phosphate removal efficiency of MEP was evaluated with the batch experiments and continuous fixed bed column reactors. On the basis of particle size and empty bed contact time (EBCT), four columns were operated for continuous 54 days. The obtained results indicated the successful application of MEP for adsorption of phosphate from an influent. Considering the potential for practical applications of the MEP, this study proposes an effective and economical method for phosphate recovery from the wastewater.

2 Materials and methods

2.1 MEP separation

The mill scale is a byproduct of an iron factory, which produces on the surface of plates/sheets during their formation by rolling red hot iron. It appears with an average diameter less than 20 mm and plate like structure. Mainly, the mill scale is composed of elemental and oxide forms of iron with small fraction of other impurities from the process such as lubricants.

The impurities were finely removed with alkaline solution in pretreatment phase (Fig. S1). For the sufficient cleaning and removal of impurities, about 10 L of 0.1 mol/L NaOH solution is used for 1 kg mill scale. Followed by alkaline cleaning, mill scale was thoroughly rinsed with deionized water and dried at 70°C (24 h). The particles were ground in Ball mill system for 3 h. The homogenized ground particles were separated with different size standard meshes (Model: 203/50 CISA, Spain). The obtained particle size was 45 to 300 μm . The schematic design of device used for separation of MEP from mill scale is presented in Fig. S2. The system is consisted of non-magnetic stainless steel plate having magnetic bars at the basement and is located at 45° angle on the stand. The stand is composed of stationary basement and two stems at one side. Springs were installed inside the stems to favor the applied force, which resulted in movement of mill scale on the plate. Different ranges of magnetic field were applied for the separation of MEP from the mill scale. Due to the strong magnetic properties, MEP are easy to isolate at low magnetic intensity. On the other hand, the weak magnetic particles (paramagnetic particles) required higher magnetic intensity field to get separate. MEP have strong attraction toward magnetic field and therefore, isolated from the diamagnetic particles under the effect of variable magnetic field intensity.

2.2 Instrumentation and chemical reagents

The batch scale adsorption experiments were performed in the Jar Tester (C-JT, Chang Shin Scientific Co., South Korea) at 250 r/min. The pH of the solutions was measured

with SevenCompact pH meter (Mettler Toledo, China) and the temperature was recorded on analytical thermometer. MEP were characterized with Powder X-ray diffraction (XRD) with Cu K α ($\lambda = 1.5406 \text{ \AA}$) radiations, operated at 40 kV and 100 mA on Rigaku D/MAX-2500/PC (Rigaku Corp. Japan). Hitachi (Japan) SU-70 field emission scanning electron micrograph (SEM) was used for the morphological investigation. The elemental composition of the MEP was recognized using Energy Dispersive X-ray spectroscopy (EDS) and X-ray Fluorescence spectrometry (XRF). Ion chromatograph (Dionex IC-5000⁺ DC, Thermo scientific, USA) was used to analyze the phosphate concentration.

All chemicals and reagents used in this study were of analytical grade and used as received. Sodium hydroxide (NaOH) and hydrochloric acid (HCl) were purchased from Fisher scientific (South Korea). Potassium phosphate monobasic (KH_2PO_4) was used to prepare phosphate solution.

2.3 Adsorption experiments

The MEP (45–75 μm size) separated at 300–500 gauss were applied as an adsorbent in batch scale experiments. The phosphate solutions of various concentrations (10–90 mg/L) were prepared in 1 L graduated glass beaker. One gram of MEP was added in each predetermined phosphate solution. The solutions were kept on stirring (250 r/min) for 24 h. Temperature and pH were controlled at 20°C and 6.5, respectively. To maintain the desire pH for the phosphate solution, 0.1 mol/L NaOH and 0.1 mol/L HCl were used. The samples obtained during experiment were filtered with 47 mm GF/C filter (WhatmanTM, 1.2 μm pore size, China) and analyzed using IC. The quantity of phosphate adsorbed onto the MEP was calculated as,

$$q_e = \frac{C_i - C_e}{m} V, \quad (1)$$

in this equation, q_e , C_i , C_e , V and m show the adsorption capacity (mg/g) at equilibrium state, initial phosphate concentrations (mg/L), equilibrium phosphate concentrations (mg/L), solution volume (mL) and mass (g) of the adsorbent (MEP), respectively. The adsorption data are also examined with Langmuir isotherm and Freundlich isotherm models that are described as Eqs. (2) and (3), respectively.

$$\frac{C_e}{q_e} = \frac{1}{q_{\max} K_L} + \frac{C_e}{q_{\max}}, \quad (2)$$

$$\ln q_e = \frac{1}{n} \ln C_e + \ln K_F, \quad (3)$$

where q_{\max} , K_L , K_F and $1/n$ are maximum adsorption capacity (mg/g), Langmuir constant (L/mg) and the Freundlich constants, respectively.

To understand the phosphate adsorption onto the MEP with respect to time, phosphate solution was prepared with 10 mg/L concentration and 1 g of MEP was added into the solution. Temperature and pH of the solution were 20°C and 6.5, respectively. The mixture was allowed to stir (250 r/min) for 2 h and the samples were collected 10 times (sampling interlude was 1–30 min) after startup. The experimental data was plotted against pseudo first order and pseudo second order kinetic models. Equations (4) and (5) represent the pseudo first order and pseudo second order kinetic model, respectively.

$$\ln(q_e - q_t) = \ln(q_e) - k_1 t, \quad (4)$$

$$\frac{t}{q_t} = \frac{1}{k_2 q_e^2} + \frac{t}{q_t}, \quad (5)$$

In above equations, q_e and q_t (mg/g) are adsorbed amount of phosphate per unit mass of adsorbent at equilibrium and time t (min), respectively. k_1 (min^{-1}) and k_2 (($\text{g}\cdot\text{mg}$)/min) are the rate constants.

The pH-dependency of phosphate adsorption onto MEP was investigated using solutions of different pH (3–11). All the solutions were prepared in 1 L graduated glass beaker and the adsorbent amount was kept constant (1 g/L). The ionic strength of the solutions was varied with addition of NaCl into the solution to achieve 0.01 and 0.1 mol/L final concentrations of NaCl into the solution. The effect of coexisting anions on the phosphate adsorption was also studied. The molar ratio of phosphate and other anions (SO_4^{2-} , NO_3^- and Cl^-) was kept 1:1. All the batch experiments were performed in triplicate.

2.4 Continuous column reactor

The phosphate adsorption behavior for MEP was also examined with continuous column operation. The column operated for present study was consist of three sections with 30 cm height (10 cm for each section). The inner diameter of the column reactor was 3 cm and the volume was calculated 212.1 cm³. The middle section of the reactor was packed with MEP attributed to packing volume 70.69 cm³ (176.7 g) and the other two sections were filled with glass beads (1–10 mm diameter). A mesh was installed between all sections to control the particle discharge. Based on particle size and EBCT, four columns were functioned (Fig. 1, Table 1). The phosphate concentration and pH of the influent stream were maintained at 2 mg/L and 6.5, respectively. The concentration of nitrate, sulfate and chloride was adjusted at 5, 6 and 110 mg/L, respectively. This concentration was set as per the anionic concentration found in influent of “S” wastewater treatment plant in South Korea. The columns were regenerated with 0.1 mol/L NaOH solution for 6 h using 1 mL/min flowrate. Followed by regeneration, MEP packed bed column reactor was thoroughly rinsed with

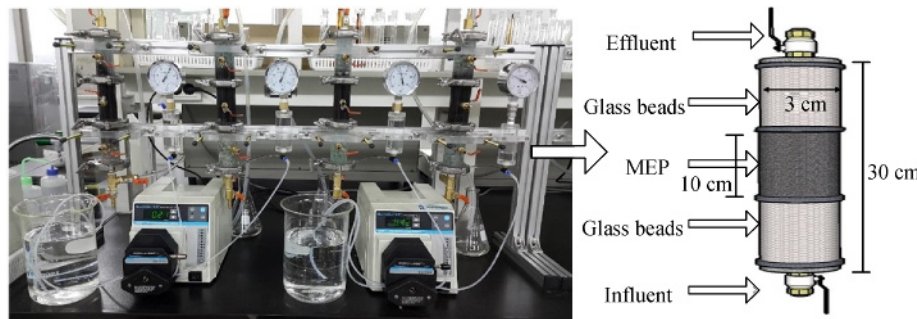


Fig. 1 Photo of the column operation with column design parameters at right side.

Table 1 Description of column operation

Period	Column	Particle size (μm)	EBCT (h)	Flow rate (L/h)
0–34 days	C1	45–75	1	0.282±0.003
	C2	75–150	1	0.285±0.003
	C3	45–75	2	0.136±0.006
	C4	75–150	2	0.142±0.007
34–50 days	C1	45–75	1	0.283±0.001
	C2	75–150	1	0.287±0.003
	C3	45–75	2	0.147±0.003
	C4	75–150	2	0.149±0.003

deionized water. The phosphate concentration in an effluent was analyzed to know the leached amount of phosphate.

3 Results and discussion

3.1 Characterization of MEP

Mill scale having size between 45 and 300 μm was used to isolate the particles having strong magnetic properties from the weaker one. Figure 2 shows the XRD pattern of the separated particles. The diffraction peaks detected at 2θ ($^{\circ}$) of 30°, 35.4°, 36.2°, 43°, 53.3°, 56.8° and 62.4° were in fine agreement with the crystalline planes of magnetite i.e., (220), (311), (222), (400), (422), (511) and (440), respectively. The close resemblance was observed between the entire XRD pattern of separated particles and the standard pattern for magnetite (JCPDS 19-0629). Similar XRD pattern was exhibited by synthesized magnetite particles (Potapova et al., 2012; Shahid et al., 2018a). The peaks at 2θ of 33°, 50° and 62.5°, attributed to hematite crystalline plane (104), (024) and (300), respectively (Asoufi et al., 2018; Funari et al., 2018). However, the diffraction peaks observed at 2θ of 42° and 61.1° were found in agreement with wustite crystalline plane i.e., (200) and (220), respectively (Yin et al., 2007). Therefore, in this study, the separated particles were quoted as MEP. The XRD pattern of MEP was found in consistent with

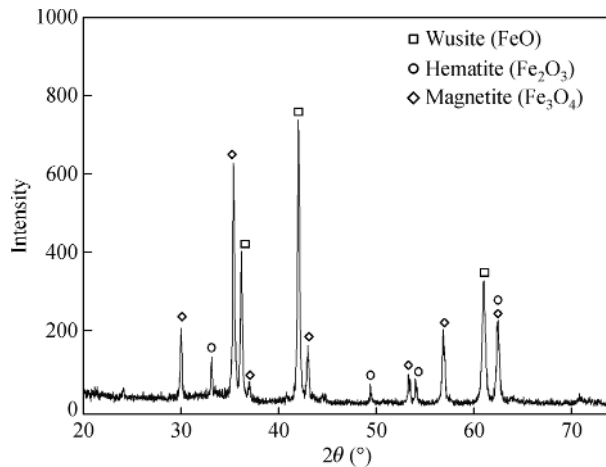


Fig. 2 XRD pattern of MEP.

various earlier studies on synthesis of ferrite particles from an iron waste (Wang and Gao, 2011; Buzin et al., 2014).

XRF analysis identified the elemental composition of MEP. The obtained data for different mesh sizes MEP is presented in Table 2. The total iron contents were found to have a major share (over 98%) among some other elemental traces. Hence, MEP used in this study has a purity of over 98.50%. It is noteworthy that the observed impurities were mainly same as identified in the natural magnetite (Alorro et al., 2010). The magnetic properties of MEP were found close to magnetite that was synthesized

Table 2 Composition (weight %) of different mesh sizes MEP as determined by XRF

Components	Weight %		
	45–75 µm	75–150 µm	150–300 µm
Fe	98.05	98.50	98.32
Mn	0.80	0.77	0.78
Cr	0.37	0.13	0.14
Cl	0.28	0.22	0.04
Si	0.16	0.12	0.35
Ni	0.15	0.03	0.03
Ca	0.09	0.10	0.08
Cu	0.03	0.05	0.04
Mo	0.03	0.04	0.03
Nb	0.02	0.03	0.03
S	—	0.02	—
Ti	0.02	—	0.03
Al	—	—	0.13

from mill scale using coprecipitation method (Fig. S3). The value of saturation magnetization for mill scale derived magnetite was 67.65 emu/g.

Surface examination and in deep elemental analysis of the MEP was done by SEM and EDS analysis, respectively. It was observed in SEM images (Fig. 3) that MEP has an irregular shape and wide-ranging size (>1 to <300 µm). Due to the van der walls forces and the magneto-dipole attraction, small particles were gathered and developed an irregular shape and size. Similar morphology of particles was observed in previous studies (Potapova et al., 2012; Salazar-Camacho et al., 2013). Several studies observed the contribution of magnetic attractions in the aggregation of magnetite nanoparticles. In an aqueous environment, an increase in surface charge of particles can enhance the repulsion between the particles and hence, hinders the aggregation of magnetite nanoparticles (Alqadami et al., 2017). The agglomerate porous and spherical appearance of separated particles observed at 500 nm scale (Fig. S4), found in consistent with previous studies (Legodi and Dewaal, 2007; Kumar et al., 2018).

Figure 4 indicates the EDS spectra of the MEP having the wide – range size. The EDS spectra confirmed the existence of oxygen and iron as the main components of MEP. The higher atomic percentage of oxygen was identified as compared with iron (Table 3). The high atomic contribution of oxygen indicates the possibility of large numbers of adsorption sites. The phosphate adsorption mechanism for the MEP is assumed to be same as discussed for iron oxides in earlier studies (Zach-Maor et al., 2011; Tofan-Lazar and Al-Abadleh, 2012; Zhang et al., 2016). The electrostatic attraction and ligand exchange mechanism are the possible pathways of phosphate

adsorption on iron oxides. The adsorption mechanism is comprehensively discussed in Sections 3.2 and 3.3.

3.2 Adsorption isotherm

The adsorption isotherm for the MEP is shown in Fig. 5. The adsorption data exhibited that an increase in initial phosphate concentration also enhances the adsorption capacity. Moreover, the solutions with low phosphate concentration attained an equilibrium state earlier than the solutions with higher concentration of phosphate. The equilibrium data was plotted in Langmuir isotherm and Freundlich isotherm models (Fig. S5) and parameters obtained from both models are given in Table 4. The model analysis of equilibrium data shows the maximum adsorption capacity of 6.414 mg/g. The value of n is determined higher than 1 that shows the fine environment for adsorption of phosphate on MEP. As compared with Freundlich isotherm, the higher value of correlation coefficient (R^2) for Langmuir isotherm shows that most of the adsorption happened on the surface layer of MEP i.e., monolayer adsorption (Wang et al., 2016; Yang et al., 2018). At the earliest stage of the experiment, rapid adsorption was observed due to the maximum accessible localities for phosphate ions. The adsorption is mostly governed by ligand exchange mechanism and electrostatic attraction between the ions (Pan et al., 2009; Yoon et al., 2018). An ion exchange reaction takes place between the phosphate ions and the hydroxyl ions present at the positively charged surface of MEP. The electrostatic properties of MEP highly depend on the hydroxyl ion concentration in the solution that may affect the interaction between MEP and phosphate ions. Earlier data discussed

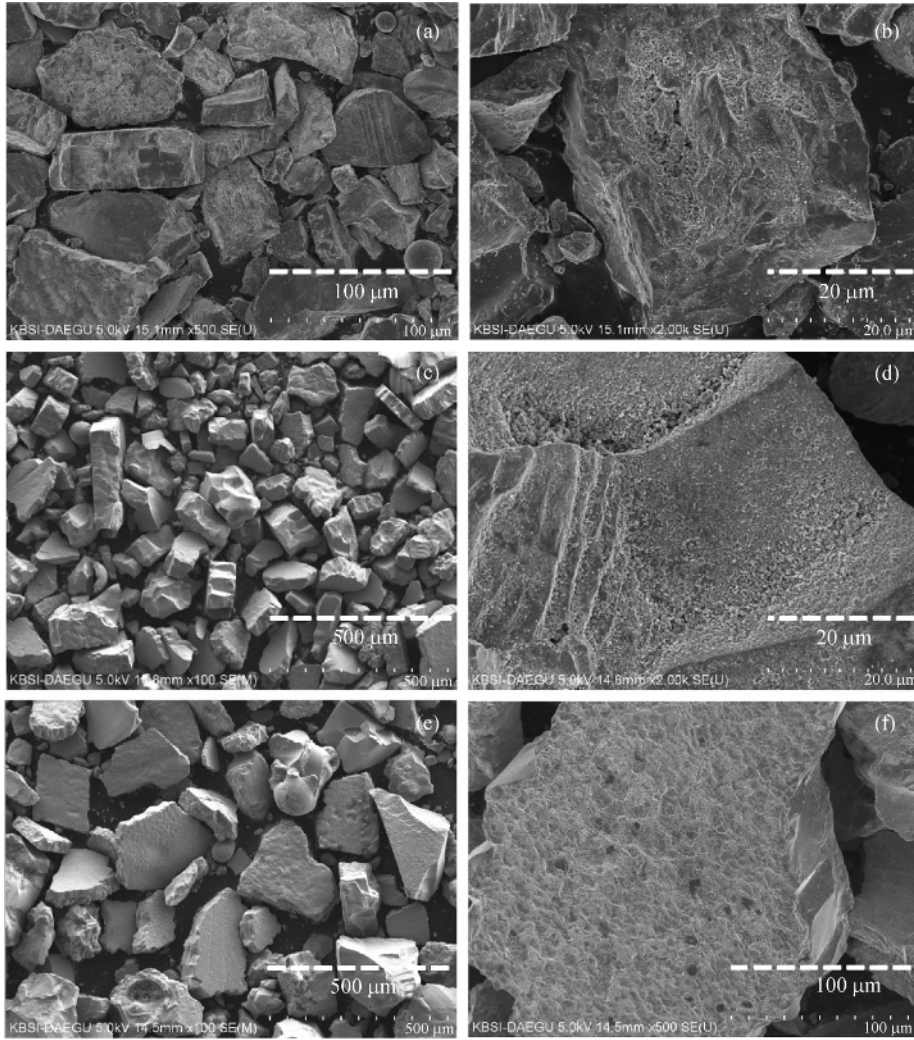


Fig. 3 SEM micrograph of MEP with wide range of size i.e., (a, b) 45–75 μm , (c, d) 75–150 μm and (e, f) 150–300 μm .

that phosphate ion has a probability to make inner-sphere complexes with mononuclear, binuclear or monodentate and bidentate complexes (Daou et al., 2007).

3.3 Adsorption kinetic

The effect of contact time for phosphate adsorption onto MEP is presented in Fig. 6. Experiment was conducted for 2 h with 10 mg/L initial concentration of phosphate. Followed by initial 2 min contact time, about 0.37 mg of phosphate was adsorbed onto the surface of MEP. After 2 h experiment, the maximum adsorption was 3.47 from the solutions having 10 mg/L initial concentration. As the experiment started, quick adsorption was observed and later, the system reached at state of equilibrium. The rapid adsorption in the beginning of the experiment might be a result of electrostatic attraction that is responsible for an enhanced moving velocity of phosphate ions toward the surface of MEP (Yang et al., 2018). At the start, phosphate

ions engaged all the accessible adsorption sites and later, started to diffuse through the internal pores of the MEP. The diffusion rate highly depends on the phosphate concentration in the solution. As the concentration of phosphate drops in the solution, the diffusion rate also drops and at the end, no more diffusion takes place and the system reaches the state of equilibrium.

Phosphate ions favor the formation of monodentate complex at the low surface coverage conditions. However, at high surface coverage, bidentate mononuclear complex might be formed. The formation of monodentate complex is a fast process as compared with bidentate complex. Moreover, in the long-term adsorption process, the transformation of monodentate complex into bidentate complex is also possible (Raven et al., 1998; Gan et al., 2018). The adsorption behavior was also studied by applying pseudo-first-order and pseudo-second-order kinetic plots for adsorption data (Fig. S6). The parameters of both models are given in Table 4. The rate constant

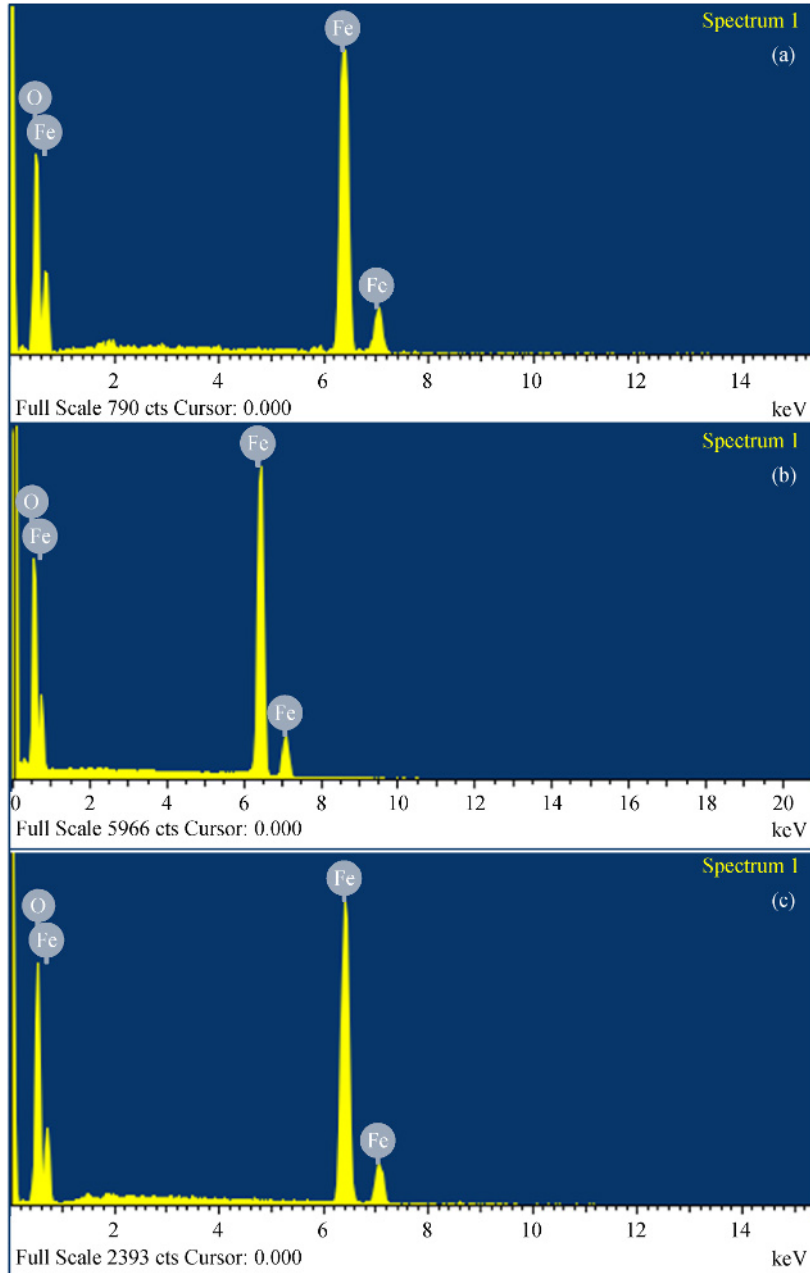


Fig. 4 EDS spectra of MEP with wide range of size i.e., (a) 45–75 μm , (b) 75–150 μm and (c) 150–300 μm .

Table 3 Elemental composition of MEP

Range of size	O	Fe
45–75 μm	58.71	41.29
75–150 μm	61.77	38.23
150–300 μm	62.13	37.87

values for k_1 and k_2 were 3.1×10^{-3} and 4×10^{-4} , respectively. The regression coefficient (R^2) value for pseudo-first-order and pseudo-second-order was 0.90 and 0.94, respectively. R^2 value indicated that adsorption

followed pseudo second order more closely that is also an indication of chemisorption. The phosphate adsorption capacity of MEP was compared with different adsorbents and presented in Table 5.

3.4 Effect of pH and ionic strength

The effect of pH and the ionic strength on the phosphate adsorption was presented in Fig. 7(a). It was observed that higher adsorption can be achieved at acidic conditions. The phosphate adsorption was quite stable at pH 6. As the pH increased, adsorption started to decrease. At basic pH, the

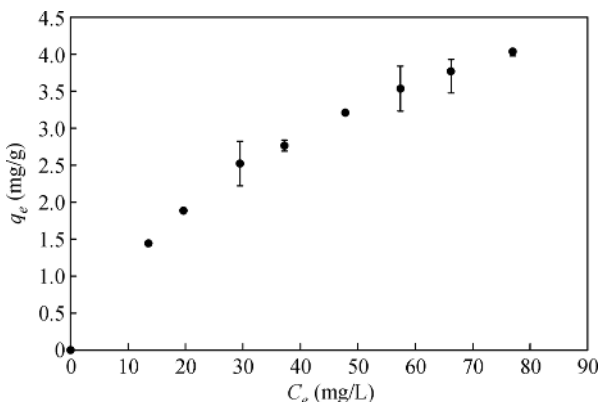


Fig. 5 Adsorption isotherm of phosphate by MEP. Error bars signify the standard deviation.

Table 4 Parameters obtained from Langmuir isotherm, Freundlich isotherm, pseudo-first-order and pseudo-second-order kinetic models for the phosphate adsorption on MEP

Model	Parameters	Value
Langmuir isotherm model	q_{\max}	6.414 mg/g
	K_L	0.021
	R^2	0.996
Freundlich isotherm model	K_F	0.329
	n	1.711
	R^2	0.993
Pseudo-first-order kinetic model	k_1	$3.1 \times 10^{-3} \text{ min}^{-1}$
	R^2	0.90
Pseudo-second-order kinetic model	k_2	$4 \times 10^{-4} (\text{g} \cdot \text{mg})/\text{min}$
	R^2	0.94

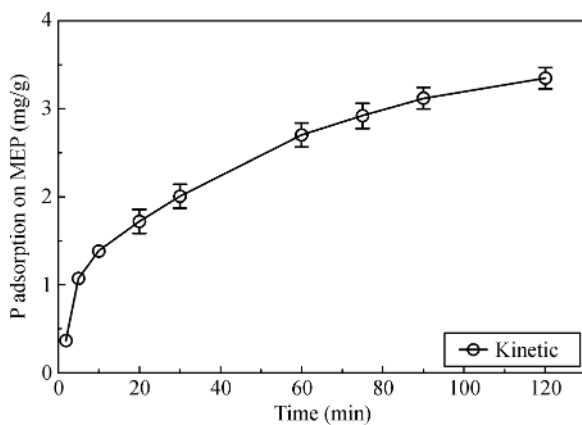


Fig. 6 Adsorption kinetics of phosphate by MEP. Error bars signify the standard deviation.

net surface charge on MEP becomes negative and causes repulsion for adjacent phosphate ions. At basic pH, the competition for sorption locations between hydroxyl and

Table 5 Phosphate adsorption capacities for different adsorbents

Adsorbent	Adsorption capacity (mg/g)	Reference
MEP	6.41	This study
Magnetic iron oxide	5.03	Yoon et al. (2014)
Magnetite based nanoparticles	5.2	Daou et al. (2007)
Agro-waste rice husk ash	0.76	Mor et al. (2016)
Polypyrrole/BOF slag nanocomposite	5.18	Islam et al. (2014)
Magnetite mineral microparticles	0.83	Xiao et al. (2017)

phosphate ions is also expected (Almasri et al., 2019). The surface charge of iron oxides remains positive below than pH 6 and negative at pH higher than 6 (Legodi and Dewaal, 2007). Any change in pH can significantly affect the net surface charge followed by a change in adsorption behavior.

Adsorption experiments were also performed in the presence of different molar concentrations of NaCl into the phosphate solution. However, ionic strength did not leave any specific effect on the phosphate removal efficiency of MEP. Figure 7(b) shows the effect of coexisting anions (NO_3^- , SO_4^{2-} and Cl^-) on the adsorptive removal of phosphate with MEP. In the presence of other anions, the phosphate adsorption behavior did not change for MEP. Phosphate ions were appeared with a higher bonding tendency toward MEP surface as compared with competing anions. Another study also supports this finding with respect to phosphate adsorption on magnetite particles (Lee and Kim, 2019). The schematic illustration of the adsorption mechanism at different pH conditions is presented in Fig. 8.

3.5 Column operation

The operational performance of MEP packed-bed columns is presented in Fig. 9. The phosphate concentration and the pH of an influent were adjusted at 2 mg/L and 6.5, respectively. The effect of an influent flowrate on phosphate removal using MEP was examined by varying the flowrate from 0.285 (1 h EBCT) to 0.142 L/h (2 h EBCT) and keeping the other conditions constant, such as pH (6.5), MEP amount (176.7 g) and phosphate concentration (2 mg/L). MEP packed-bed columns were found successful to remove phosphate concentration from an influent stream. The breakthrough curves showed that the phosphate adsorption on MEP increases with decreasing flowrate. The high contact time between phosphate solution and the MEP packed-bed column is the major reason for better adsorption at low flowrate. Columns 1 and 2 (1 h EBCT) were regenerated with 0.1 mol/L NaOH after continuous operation for 34 days. The adsorption capacity of both columns was finely restored at initial state after regeneration. However, columns 3 and 4 were successfully

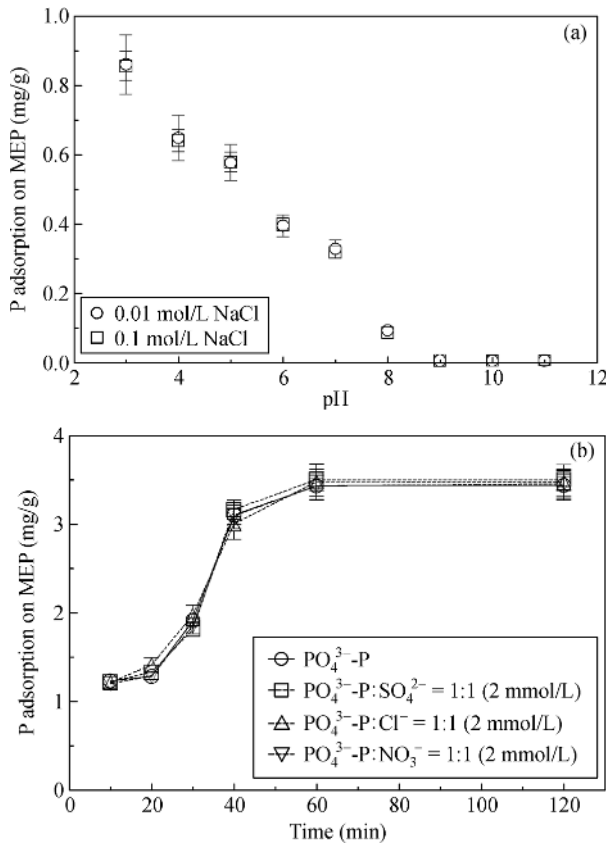


Fig. 7 Effect of pH and ionic strength on phosphate adsorption (a) and the effect of coexisting anions (b) on phosphate adsorption. Error bars signify the standard deviation

operated without regeneration for 54 days. Based on the entire operation, it can be stated that a column packed with MEP can effectively remove the phosphate concentration

from contaminated water for more than 7 weeks. Moreover, no crack or blockage was observed in a column during the entire operation. Lastly, based on column operation, it can be stated that up to 2 mg/L initial phosphate concentration of solution can effectively remove in continuous operation and an alkaline cleaning can efficaciously desorb over 90% of the adsorbed amount of phosphate onto the surface of MEP.

The morphological examination of used particles confirmed the adsorption of phosphate onto the surface of MEP. As shown in Fig. 10, the significant morphological changes were observed in MEP. The needle like structure was appeared in SEM analysis that was found similar to previously reported phosphate loaded iron particles (Pramanik et al., 2015). The gathering of needle like structure also appeared in the form of bright patches at some places that was found in consistent with an earlier study reported on phosphate adsorption (Islam et al., 2014). Furthermore, the EDS spectra of phosphate loaded MEP also confirmed the existence of phosphorus in MEP. The identification of P in EDS spectra also indicates the contribution of chemical adsorption during phosphate adsorption process. This finding also supports the adsorption mechanism that was discussed in Sections 3.2 and 3.3.

4 Conclusions

This study introduces MEP, a newly formed adsorbent for phosphate recovery from wastewater. A new method and device were introduced for the separation of MEP. MEP were isolated from mill scale under the effect of variable magnetic field intensity. Separated particles were characterized by a number of techniques like XRF, XRD, SEM

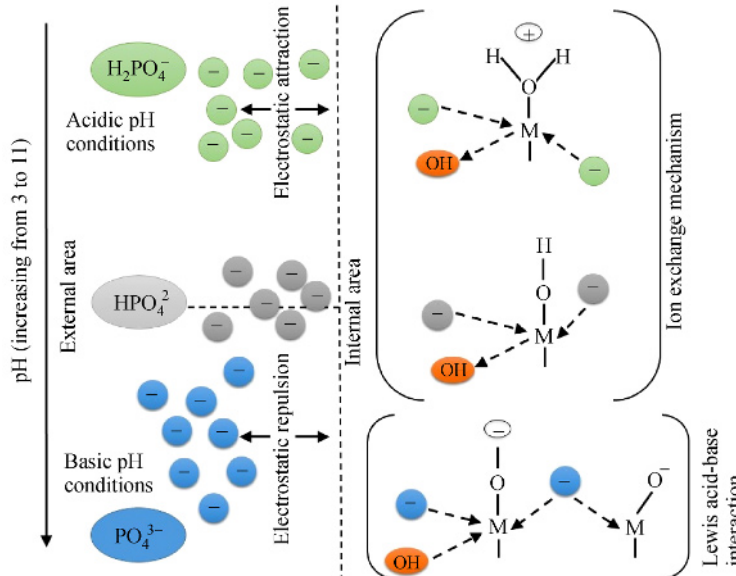


Fig. 8 The schematic illustration of phosphate adsorption on MEP.

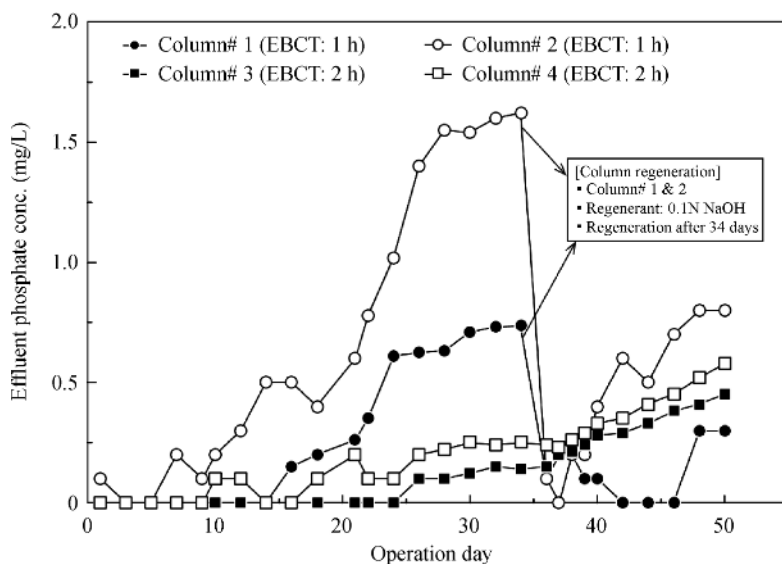


Fig. 9 The operational behavior of columns.

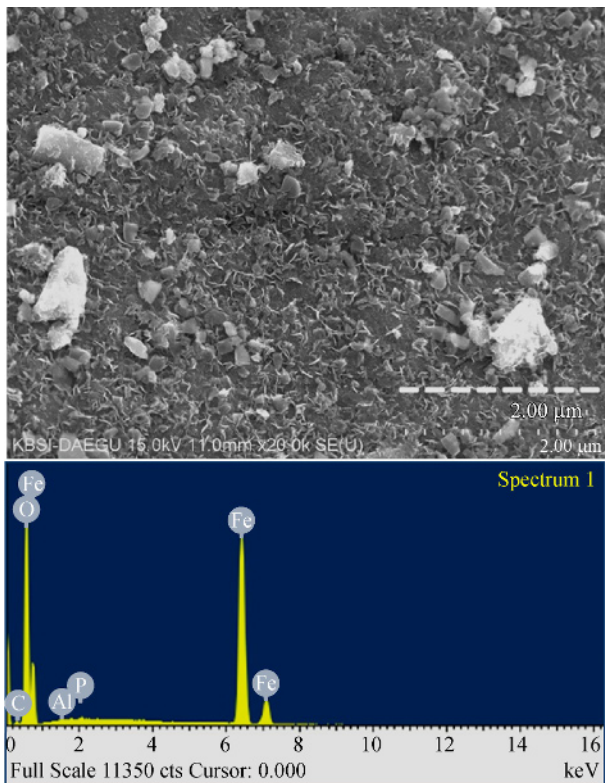


Fig. 10 The SEM image and EDS spectra of MEP after phosphate adsorption.

and EDS. The XRD pattern of MEP indicated the crystalline planes of magnetite i.e., (220), (311), (222), (400), (422), (511) and (440). The elemental analysis confirmed over 98% purity in composition. The agglomerate porous morphology of magnetite is confirmed during

morphological investigation of MEP. The adsorption data was well explained using Langmuir isotherm, Freundlich isotherm, pseudo-first-order and pseudo-second-order kinetic models, indicating the monolayer phosphate adsorption onto the MEP. The phosphate adsorption capacity for MEP was determined 6.41. Based on EBCT (1 and 2 h) and particle size (45–75 and 75–150 μm), four column reactors were operated for 54 days. The column operated at slow flowrate explored the higher sorption rate because of greater contact time between MEP and phosphate ions. The regeneration of columns with 0.1 mol/L NaOH solution was found effective for enhancing the adsorption behavior of MEP in long-term operation. Based on this study, an economical, effective and ecofriendly method is suggested for the separation of MEP from mill scale and its application for adsorptive removal of phosphate from the contaminated water.

Acknowledgements This work was supported by 2015 Advanced Industrial Technology Development program by the Ministry of Environment (MOE), Republic of Korea (Project 2015000150006).

Electronic Supplementary Material Supplementary material is available in the online version of this article at <https://doi.org/10.1007/s11783-019-1151-2> and is accessible for authorized users.

References

- Almasri D A, Saleh N B, Atieh M A, McKay G, Ahzi S (2019). Adsorption of phosphate on iron oxide doped halloysite nanotubes. *Scientific Reports*, 9(1): 3232
- Alorro R D, Hiroyoshi N, Kijitani H, Ito M, Tsunekawa M (2010). On the use of magnetite for gold recovery from chloride solution. *Mineral Processing and Extractive Metallurgy Review*, 31(4): 201–213

- Alqadami A A, Naushad M, Abdalla M A, Ahamed T, Alothman Z A, Alshehri S M, Ghfar A A (2017). Efficient removal of toxic metal ions from wastewater using a recyclable nanocomposite: A study of adsorption parameters and interaction mechanism. *Journal of Cleaner Production*, 156: 426–436
- Asoufi H M, Al-Antary T M, Awwad A M (2018). Green route for synthesis hematite (α -Fe₂O₃) nanoparticles: Toxicity effect on the green peach aphid, *Myzus persicae* (Sulzer). *Environmental Nanotechnology, Monitoring & Management*, 9: 107–111
- Buzin P G W K D, Vigânico E M, Silva R D A, Heck N C, Schneider I A, Menezes J C S (2014). Production of ferrous sulfate from steelmaking mill scale. *International Journal of Scientific and Engineering Research*, 5(4): 353–359
- Daou T J, Begin-Colin S, Grenèche J M, Thomas F, Derory A, Bernhardt P, Legaré P, Pourroy G (2007). Phosphate adsorption properties of magnetite-based nanoparticles. *Chemistry of Materials*, 19(18): 4494–4505
- Funari V, Mantovani L, Vigliotti L, Tribaudino M, Dinelli E, Braga R (2018). Superparamagnetic iron oxides nanoparticles from municipal solid waste incinerators. *Science of the Total Environment*, 621: 687–696
- Gan L, Lu Z, Cao D, Chen Z (2018). Effects of cetyltrimethylammonium bromide on the morphology of green synthesized Fe₃O₄ nanoparticles used to remove phosphate. *Materials Science and Engineering C*, 82: 41–45
- Guaya D, Valderrama C, Farran A, Sauras T, Cortina J L (2018). Valorisation of N and P from waste water by using natural reactive hybrid sorbents: Nutrients (N,P,K) release evaluation in amended soils by dynamic experiments. *Science of the Total Environment*, 612: 728–738
- Gypser S, Hirsch F, Schleicher A M, Freese D (2018). Impact of crystalline and amorphous iron- and aluminum hydroxides on mechanisms of phosphate adsorption and desorption. *Journal of Environmental Sciences-China*, 70: 175–189
- Huang W, Zhang Y, Li D (2017). Adsorptive removal of phosphate from water using mesoporous materials: A review. *Journal of Environmental Management*, 193: 470–482
- Islam M, Mishra S, Swain S K, Patel R, Dey R K, Naushad M (2014). Evaluation of phosphate removal efficiency from aqueous solution by polypyrrole/BOF slag nanocomposite. *Separation Science and Technology*, 49(17): 2668–2680
- Khafri H Z, Ghaedi M, Asfaram A, Safarpoor M (2017). Synthesis and characterization of ZnS:Ni-NPs loaded on AC derived from apple tree wood and their applicability for the ultrasound assisted comparative adsorption of cationic dyes based on the experimental design. *Ultrasonics Sonochemistry*, 38: 371–380
- Kumar A, Kumar A, Sharma G, Al-Muhtaseb A H, Naushad M, Ghfar A A, Stadler F J (2018). Quaternary magnetic BiOCl/g-C₃N₄/Cu₂O/Fe₃O₄ nano-junction for visible light and solar powered degradation of sulfamethoxazole from aqueous environment. *Chemical Engineering Journal*, 334: 462–478
- Lee W H, Kim J O (2019). Effect of coexisting components on phosphate adsorption using magnetite particles in water. *Environmental Science and Pollution Research International*, 26(2): 1054–1060
- Legodi M, Dewaal D (2007). The preparation of magnetite, goethite, hematite and maghemite of pigment quality from mill scale iron waste. *Dyes and Pigments*, 74(1): 161–168
- Li F, Wang L, Ji C, Wu H, Zhao J, Tang J (2017). Toxicological effects of tris(2-chloropropyl) phosphate in human hepatic cells. *Chemosphere*, 187: 88–96
- Li Z, Qiu Z, Yang J, Ma B, Lu S, Qin C (2018). Investigation of phosphate adsorption from an aqueous solution using spent fluid catalytic cracking catalyst containing lanthanum. *Frontiers of Environmental Science & Engineering*, 12(6): 15
- Mor S, Chhoden K, Ravindra K (2016). Application of agro-waste rice husk ash for the removal of phosphate from the wastewater. *Journal of Cleaner Production*, 129: 673–680
- Ngo H H, Guo W (2009). Membrane fouling control and enhanced phosphorus removal in an aerated submerged membrane bioreactor using modified green bioflocculant. *Bioresource Technology*, 100 (18): 4289–4291
- Nohra J S A, Madramootoo C A, Hendershot W H (2007). Modelling phosphate adsorption to the soil: application of the non-ideal competitive adsorption model. *Environmental Pollution*, 149(1): 1–9
- Pan B, Wu J, Pan B, Lv L, Zhang W, Xiao L, Wang X, Tao X, Zheng S (2009). Development of polymer-based nanosized hydrated ferric oxides (HFOs) for enhanced phosphate removal from waste effluents. *Water Research*, 43(17): 4421–4429
- Potapova E, Yang X, Westerstrand M, Grahn M, Holmgren A, Hedlund J (2012). Interfacial properties of natural magnetite particles compared with their synthetic analogue. *Minerals Engineering*, 36–38: 187–194
- Pramanik M, Imura M, Lin J, Kim J, Kim J H, Yamauchi Y (2015). Shape-controlled synthesis of mesoporous iron phosphate materials with crystallized frameworks. *Chemical Communications (Cambridge)*, 51(72): 13806–13809
- Rashid M, Price N T, Gracia Pinilla M A, O’Shea K E (2017). Effective removal of phosphate from aqueous solution using humic acid coated magnetite nanoparticles. *Water Research*, 123: 353–360
- Raven K P, Jain A, Loepert R H (1998). Arsenite and arsenate adsorption on ferrihydrite Kinetics, equilibrium, and adsorption envelopes. *Environmental Science & Technology*, 32(3): 344–349
- Salazar-Camacho C, Villalobos M, Rivas-Sánchez M D L L, Arenas-Alatorre J, Alcaraz-Cienfuegos J, Gutiérrez-Ruiz M E (2013). Characterization and surface reactivity of natural and synthetic magnetites. *Chemical Geology*, 347: 233–245
- Shahid M K, Choi Y G (2018). The comparative study for scale inhibition on surface of RO membranes in wastewater reclamation: CO₂ purging versus three different antiscalants. *Journal of Membrane Science*, 546: 61–69
- Shahid M K, Kim J Y, Choi Y G (2019a). Synthesis of bone char from cattle bones and its application for fluoride removal from the contaminated water. *Groundwater for Sustainable Development*, 8: 324–331
- Shahid M K, Phearom S, Choi Y G (2018a). Synthesis of magnetite from raw mill scale and its application for arsenate adsorption from contaminated water. *Chemosphere*, 203: 90–95
- Shahid M K, Phearom S, Choi Y G (2019b). Evaluation of arsenate adsorption efficiency of mill-scale derived magnetite particles with column and plug flow reactors. *Journal of Water Process Engineering*, 28: 260–268
- Shahid M K, Pyo M, Choi Y G (2017). Carbonate scale reduction in

- reverse osmosis membrane by CO₂ in wastewater reclamation. *Membrane Water Treatment*, 8(2): 125–136
- Shahid M K, Pyo M, Choi Y G (2018b). The operation of reverse osmosis system with CO₂ as a scale inhibitor: A study on operational behavior and membrane morphology. *Desalination*, 426: 11–20
- Tofan-Lazar J, Al-Abadleh H A (2012). ATR-FTIR studies on the adsorption/desorption kinetics of dimethylarsinic acid on iron-(oxyhydr)oxides. *Journal of Physical Chemistry A*, 116(6): 1596–1604
- Vikrant K, Kim K H, Ok Y S, Tsang D C W, Tsang Y F, Giri B S, Singh R S (2018). Engineered/designer biochar for the removal of phosphate in water and wastewater. *Science of the Total Environment*, 616–617: 1242–1260
- Wang L, Gao L (2011). Controlled synthesis and tunable properties of hematite hierarchical structures in a dual-surfactant system. *CrystEngComm*, 13(6): 1998–2005
- Wang Z, Shen D, Shen F, Li T (2016). Phosphate adsorption on lanthanum loaded biochar. *Chemosphere*, 150: 1–7
- Xiao X, Liu S, Zhang X, Zheng S (2017). Phosphorus removal and recovery from secondary effluent in sewage treatment plant by magnetite mineral microparticles. *Powder Technology*, 306: 68–73
- Yang B, Liu D, Lu J, Meng X, Sun Y (2018). Phosphate uptake behavior and mechanism analysis of facilely synthesized nanocrystalline Zn-Fe layered double hydroxide with chloride intercalation. *Surface and Interface Analysis*, 50(3): 378–392
- Ye F, Li Y, Lin Q, Zhan Y (2017). Modeling of China's cassava-based bioethanol supply chain operation and coordination. *Energy*, 120: 217–228
- Yin M, Chen Z, Deegan B, O'brien S (2007). Wüstite nanocrystals: Synthesis, structure and superlattice formation. *Journal of Materials Research*, 22(7): 1987–1995
- Yoon H S, Chung K W, Kim C J, Kim J H, Lee H S, Kim S J, Lee S I, Yoo S J, Lim B C (2018). Characteristics of phosphate adsorption on ferric hydroxide synthesized from a Fe₂(SO₄)₃ aqueous solution discharged from a hydrometallurgical process. *Korean Journal of Chemical Engineering*, 35(2): 470–478
- Yoon S Y, Lee C G, Park J A, Kim J H, Kim S B, Lee S H, Choi J W (2014). Kinetic, equilibrium and thermodynamic studies for phosphate adsorption to magnetic iron oxide nanoparticles. *Chemical Engineering Journal*, 236: 341–347
- Zach-Maor A, Semiat R, Shemer H (2011). Adsorption-desorption mechanism of phosphate by immobilized nano-sized magnetite layer: Interface and bulk interactions. *Journal of Colloid and Interface Science*, 363(2): 608–614
- Zhang L, Gao Y, Xu Y, Liu J (2016). Different performances and mechanisms of phosphate adsorption onto metal oxides and metal hydroxides: a comparative study. *Journal of Chemical Technology and Biotechnology* (Oxford, Oxfordshire), 91(5): 1232–1239
- Zhang T, Xu H, Li H, He X, Shi Y, Kruse A (2018). Microwave digestion-assisted HFO/biochar adsorption to recover phosphorus from swine manure. *Science of the Total Environment*, 621: 1512–1526